Supporting Information

Synergistic Non-covalent Recognition Enabled Highly Efficient Through-space Charge Transfer for Specific Synthetic Cannabinoid EG-2201 Detection

Liwei Tang[a], Chuanfang Zhao[b], Jiahao Dong[b], Turghun Muhammad[a], Jiajia Fan[b],*

Xincun Dou[a, b, c], Yuan Liu*[b]*

[a] College of Chemistry, Xinjiang University, Urumqi 830017, China

[b] Xinjiang Key Laboratory of Trace Chemical Substances Sensing, Xinjiang Joint Laboratory of Illicit Drugs Control, Xinjiang Technical Institute of Physics & Chemistry, Chinese Academy of Sciences, Urumqi 830011, China

[c] Center of Materials Science and Optoelectronics Engineering, University of Chinese Academy of Sciences, Beijing 100049, China

1 Experimental Section

1.1 Chemicals and Measurement

Unless otherwise noted, all reagents and materials were obtained from commercial sources without further purification. 4-bromo-1,8-naphthalene anhydride, carbazole, and naphthalene were purchased from Adamas (Shanghai, China). Methyl isothiocyanate, allylamine hydrochloride and glycine were purchased from Aladdin (Shanghai, China). Ethanol (EtOH), methanol (MeOH), 1,4-Dioxane (Diox), Acetonitrile (ACN), 1,2-propanediol and glycerol were purchased from Xinbrete (Tianjin, China). Hydrazine and hydrochloric acid were purchased from Sinopharm (Shanghai, China). N,N-dimethylformamide (DMF) and dimethyl sulfoxide (DMSO) were purchased from Damas-beta (Shanghai, China). Barbital, fentanyl, etonitazene, etomidate, tetrahydrocannabinol, synthetic cannabinoids (EG-2201, JWH-018, AM-2201, MDMB-CHMCZCA, 5F-MDMB-PICA, MDMB-CHMINCA) were purchased from Yuansi (Shanghai, China). E-liquid, petals, sucrose and tobacco leaves were purchased commercially, while urine was from the volunteer. Silicon-based fibrous film was purchased from Jiening (Shanghai, China).

By using the tetramethyl silane as the internal standard, 1H nuclear magnetic resonance (NMR) spectra were measured on a high resolution 400 MHz superconducting NMR spectrometer (Burker, Germany). Mass spectra were determined with a Q Exactive-type four-stage rod orbitrap high resolution mass spectrometer (HRMS, UHPLC-Q-Orbitrap-HRMS, Thermo Fisher Scientific, USA). The fluorescence spectra were collected on an Edinburgh FLS1000 fluorescence spectrophotometer (Edinburgh Instruments, UK). The sensing images were obtained by an iPhone 15 Pro Max (Apple Inc., USA). Attenuated total reflection Flourier transformed infrared (ATR-FTIR) spectra were obtained by using a PerkinElmer Frontier with a universal ATR sampling accessory from PerkinElmer (PerkinElmer, Japan).

1.2 Synthetic details

Synthesis of 2-(6-Bromo-1,3-dioxo-1H-benzo[de]isoquinolin-2(3H)-yl) acetic acid

A mixture of 4-bromo-1,8-naphthalic anhydride (1.1123 g), glycine (0.3426 g), and triethylamine (0.504 g) in anhydrous EtOH (30 mL) was heated under reflux at 80 °C for 8 hours. After cooling to room temperature, the reaction mixture was acidified by adding 1 M hydrochloric acid solution (5 mL), resulting in the formation of a white precipitate. The precipitate was collected by suction filtration, washed thoroughly with water and anhydrous ethanol (six times), and dried in vacuum to afford the compound as a white solid in 80% yield. 1H NMR (400 MHz, dmso) δ 8.57 (td, J = 7.3, 1.1 Hz, 2H), 8.34 (d, J = 7.9 Hz, 1H), 8.22 (d, J = 7.9 Hz, 1H), 8.00 (dd, J = 8.5, 7.3 Hz, 1H), 4.71 (s, 2H).

Synthesis of 2-(6-(2-(Methylcarbamothioyl)hydrazinyl)-1,3-dioxo-1H-benzo[de]isoquinolin-2(3H)-

yl)acetic acid (COOH-Naph)

2-(6-bromo-1,3-dioxo-1H-benzo[de]isoquinolin-2(3H)-yl) acetic acid (0.6231 g) in anhydrous EtOH (75 mL) was treated with hydrazine hydrate (6 mL). The reaction was stirred and heated under reflux at 85 °C for 4 hours under a nitrogen atmosphere. Upon cooling, the resulting precipitate was isolated by filtration, washed successively with DCM, PE and EtOH, and dried in vacuum to yield the yellow solid. A solution of the above yellow solid (0.4673 g) and methyl isothiocyanate (0.1902 g) in anhydrous EtOH (60 mL) was heated under reflux at 80 °C for 24 hours. After cooling, the precipitate was collected by filtration, washed with cold anhydrous ethanol, then, dried in vacuum to obtain the final product, the probe 1 (COOH-Naph), as a solid in 56% yield. ^{1}H NMR (400 MHz, dmso) δ 9.73 (s, 2H), 8.68 (d, *J* = 8.5 Hz, 1H), 8.49 (d, *J* = 7.2 Hz, 1H), 8.37 (d, *J* = 8.4 Hz, 2H), 7.77 (t, *J* = 7.9 Hz, 1H), 6.87 (d, *J* = 8.4 Hz, 1H), 4.67 (s, 2H), 2.87 (d, *J* = 4.3 Hz, 3H). HRMS: [M] + Calcd. for 358.07; Found 359.08.

Synthesis of 2-allyl-6-bromo-1H-benzo[de]isoquinoline-1,3(2H)-dione

A mixture of 4-bromo-1,8-naphthalic anhydride (1.4756 g), allylamine hydrochloride (0.8924 g), and triethylamine (2.5mL) in anhydrous EtOH (60 mL) was heated under reflux at 80 °C for 8 hours. The reaction solution was directly poured into 250 mL ice water and purified by column chromatography with the eluent of PE:EA = 20:1 to afford a yellow solid in 72% yield. ^{1}H NMR (400 MHz, dmso) δ 8.51 (ddd, *J* = 9.6, 7.9, 1.1 Hz, 2H), 8.30 – 8.16 (m, 2H), 7.96 (dd, *J* = 8.5, 7.3 Hz, 1H), 5.91 (ddt, *J* = 17.2, 10.4, 5.2 Hz, 1H), 5.19 – 5.09 (m, 2H), 4.62 (dd, *J* = 5.3, 1.6 Hz, 2H).

Synthesis of 2-(2-allyl-1,3-dioxo-2,3-dihydro-1H-benzo[de]isoquinolin-6-yl)-N-methylhydrazine-1-carbothioamide (DB-Naph)

2-allyl-6-bromo-1H-benzo[de]isoquinoline-1,3(2H)-dione (0.6547 g) in anhydrous EtOH (50 mL) was treated with hydrazine hydrate (2.5 mL). The reaction was stirred and heated under reflux at 85 °C for 4 hours under a nitrogen atmosphere. Upon cooling, the resulting precipitate was isolated by filtration, washed successively with DCM, PE and EtOH, and dried in vacuum to yield the yellow solid. A solution of the above yellow solid (0.1904 g) and methyl isothiocyanate (0.1916 g) in anhydrous EtOH (30 mL) was heated under reflux at 80 °C for 24 hours. After cooling, the precipitate was collected by filtration, washed with cold anhydrous ethanol, then, dried in vacuum to obtain the final product, the probe 2 (DB-Naph), as a solid in 50% yield. ^{1}H NMR (400 MHz, dmso) δ 9.71 (d, *J* = 15.5 Hz, 2H), 8.71 – 8.61 (m, 1H), 8.50 – 8.41 (m, 1H), 7.79 – 7.72 (m, 1H), 6.86 (d, *J* = 8.4 Hz, 1H), 5.91 (ddt, *J* = 17.0, 10.5, 5.2 Hz, 1H), 5.09 – 4.90 (m, 2H), 4.62 (dt, *J* = 5.2, 1.7 Hz, 2H), 2.87 (d, *J* = 4.4 Hz, 3H).

1.3 Theoretical calculations

The ground-state geometry was optimized using the hybrid density functional PBE0 with Grimme's DFT-D3(BJ) empirical dispersion correction[1-4]. The def2-svp basis set was employed for all atoms, and

excited-state optimization was conducted at the TD-PBE0-D3(BJ)/def2-svp level of theory[5]. The PCM solvent model was employed to simulate the solvent environment of DMSO and study solvent effects[6-7]. Further frequency calculations on the optimized geometries were performed at the same level of theory to ensure no imaginary frequencies were present. To get more precise binding energies, the single point energies were calculated with wb97xd/def2tzvp method and PCM solvation model on their optimized structures[8-9]. Quantum chemical calculations were performed using the Gaussian 16C.01 package[10]. In analyzing the electrostatic potential (ESP) on the van der Waals (vdW) surface, we referred to Bader's definition, utilizing the vdW surface at the isovalue of q = 0.001 a.u. Non-covalent intermolecular interactions (*e.g.*, π-π stacking) were investigated using the Independent Gradient Model (IGM) theory based on molecular density[11]. The intermolecular weak interactions were visualized through colored isosurface maps. Based on the IGM theory, we introduced the scatter plot of δg and sign (λ2)ρ to quantitatively analyze the strength of intermolecular weak interactions, where green represents van der Waals interactions and blue indicates hydrogen bonding interactions. Unless otherwise specified, all wavefunction analyses (HOMO-LUMO, ESP, IGM, electron-hole, etc.) and the generation of various isosurface maps were carried out using the Multiwfn 3.8 (dev) software[12-13]. The files exported from Multiwfn were then used to generate isosurface maps with the VMD visualization program[14].

1.4 Testing process

Optimization of solvents for Naph

The COOH-Naph and DB-Naph were separately dispersed in various solvents (DMSO, DMF, MeOH, Diox, THF, and can) with a concentration of 0.02 mg/mL. Afterwards, 40 μL EG-2201 with a concentration of 1 mg/mL was added to 160 μL probe solutions, respectively. The fluorescence spectra of the COOH-Naph and DB-Naph solutions before and after adding EG-2201 were collected by using the Edinburgh FLS1000 fluorescence spectrophotometer with parameters of λ_{ex}= 365 nm, excitation slit: 2 nm; emission slit: 1.5 nm. All optical images were recorded using the iPhone 15 Pro Max smartphone under a 365 nm illumination.

Sensitivity study

150 μL EG-2201 solution with concentrations of 114.0, 130.2, 146.5, 162.8, 179.1, 195.4, 211.6, 227.9, 244.2 and 260.5 μM was added to 150 μL 0.1 mg/mL COOH-Naph solution, respectively. Then, the fluorescence spectra and optical images were recorded under the same condition as above mentioned.

Specificity study and anti-interference study

To investigate the specificity and anti-interference capability of the COOH-Naph towards EG-2201, 15 substances, including conventional drugs (THC, barbital, fentanyl, etonitazene, etomidate), structural analogues (JWH-018, AM-2201, MDMB-CHMCZCA, 5F-MDMB-PICA, MDMB-CHMINCA,

carbazole, naphthalene) and additives (sucrose, 1,2-propanediol, glycerine) were selected as potential interfering substances.

For the specificity study, 150 μL the above-mentioned potential interfering substances at a concentration of 2 mM and EG-2201 at a concentration of 0.2 mM was separately added to 150 μL 0.02 mg/mL COOH-Naph solution. Then, the fluorescence spectra and optical images were recorded under the same condition as above mentioned.

In terms of anti-interference study, 75 μL 4 mM the aforementioned potential interfering substance was mixed with 75 μL 0.4 mM EG-2201. Then, the mixture which includes both EG-2201 and potential interfering substance was added to 150 μL 0.02 mg/mL COOH-Naph solution. Then, the fluorescence spectra and optical images were recorded under the same condition as above mentioned.

Preparation of simulated samples

100 μL 0.2 mM EG-2201 was added in the urine and E-liquid, or sprayed onto tobacco and petals as the simulated samples. Then, 100 μL liquidous sample was dropped into 100 μL COOH-Naph solution, then, the fluorescence image would be recorded under 365 nm illumination by using the iPhone 15 Pro Max smartphone.

Spike recovery experience

150 μL probe solution, 17 μL EG-2201, 123 μL MeOH, and 10 μL E-liquid were mixed to prepare an E-liquid sample with an EG-2201 concentration of 140 μM. 150 μL probe solution, 17 μL EG-2201, 123 μL MeOH, and 10 μL urine were mixed to prepare an urine sample with an EG-2201 concentration of 140 μM. 150 μL of probe solution, 26 μL of EG-2201, 124 μL of MeOH, and 5 mg petals were mixed to prepare a petals sample with an EG-2201 concentration of 210 μM. 150 μL of probe solution, 26 μL of EG-2201, 124 μL of MeOH, and 5 mg tobacco were mixed to prepare a tobacco sample with an EG-2201 concentration of 210 μM. Three parallel experiments were performed for each sample group. Then, the fluorescence spectra was recorded under the same condition as above mentioned.

Functionalized sensing film preparation

Silicon-based fibrous film was immersed in a 0.1 mg/mL COOH-Naph solution for 10 min, and then was air-dried and placed into a unit of sensing chip of the analyzer. Pure methanol and EG-2201-methanol solution were separately dropped onto this unit as the negative (-) and positive (+) samples, respectively. The analyzer was used to discriminate the two groups *via* the hue-saturation-value (HSV) ranges, with the negative control exhibiting H: 120-160, S: 0.4-0.6, V: 0.5-1 and the positive group showing H: 90-145, S: 0.1-0.4, V: 0.3-0.5. Then, an alarm would be automatically triggered by the analyzer when the HSV values of test samples fell into the positive control range. Similarly, the RGB values were also used for double-checking the discrimination while the R, G, B values were located in the ranges of 50-114, 77-

127 and 11-57, respectively.

1.5 S/N value calculation

According to the following formulas, the S/N value is obtained.

$$SNR = \frac{\left|I_{\text{sample}} - \overline{I_{\text{blank}}}\right|}{SD_{\text{blank}}} = \frac{\left|I_{sample} - \overline{I_{blank}}\right|}{\sqrt{\frac{1}{n-1}\sum_{i=1}^{n}\left(I_{blank,i} - \overline{I_{blank}}\right)^2}}$$

2 Supplementary figures

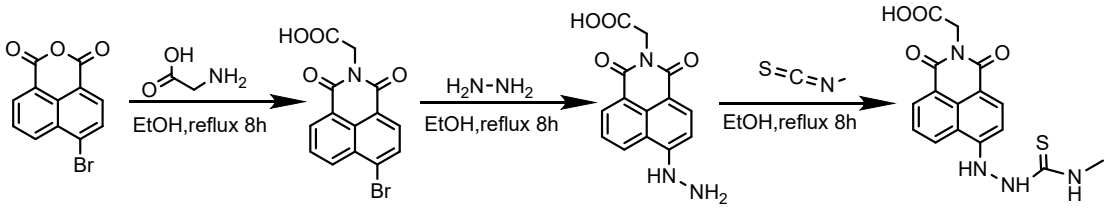

Figure S1. Synthetic procedures of COOH-Naph.

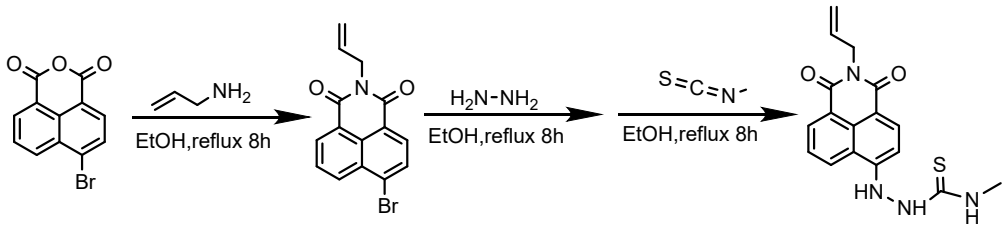

Figure S2. Synthetic procedures of DB-Naph.

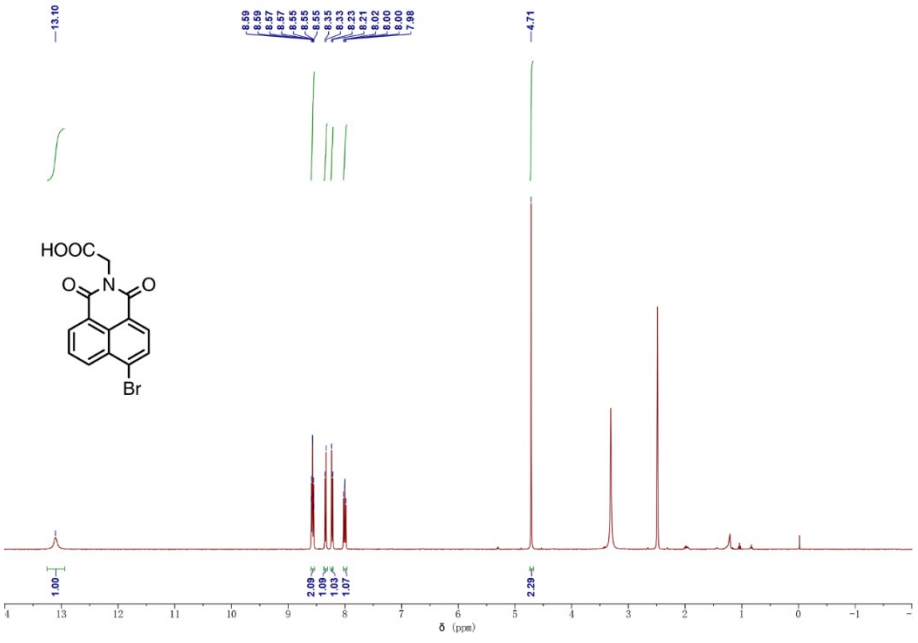

Figure S3. ^{1}H NMR spectrum of 2-(6-Bromo-1,3-dioxo-1H-benzo[de]isoquinolin-2(3H)-yl) acetic acid (DMSO, 400 MHz, 298 K).

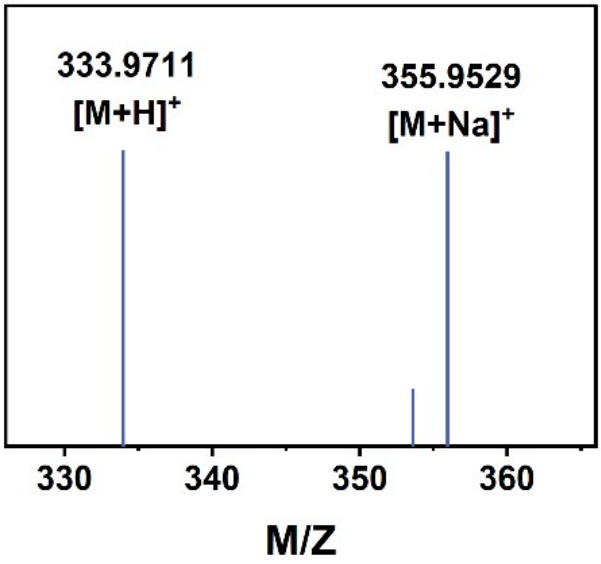

Figure S4. HRMS spectrum of 2-(6-Bromo-1,3-dioxo-1H-benzo[de]isoquinolin-2(3H)-yl) acetic acid.

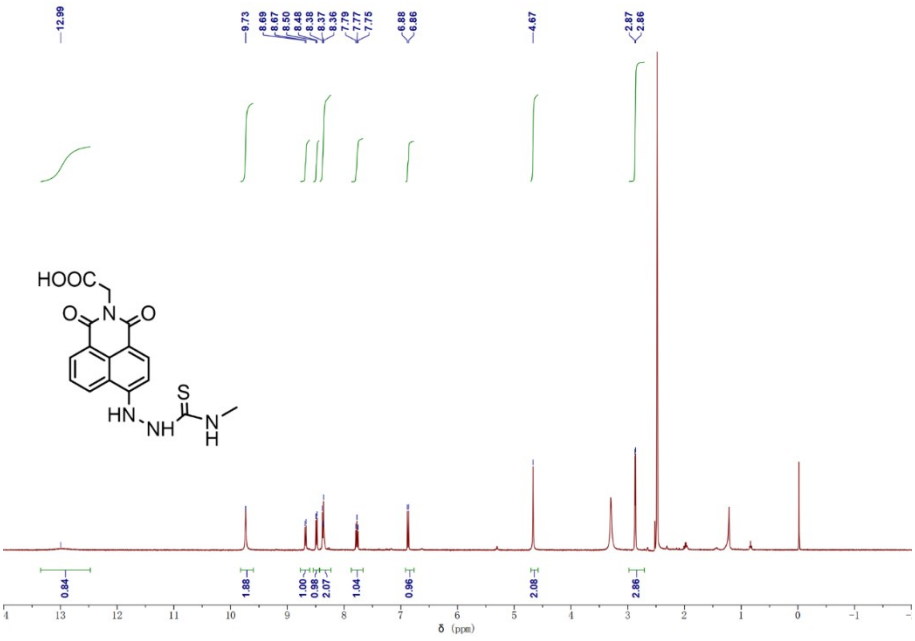

Figure S5. ^{1}H NMR spectrum of COOH-Naph (DMSO, 400 MHz, 298 K).

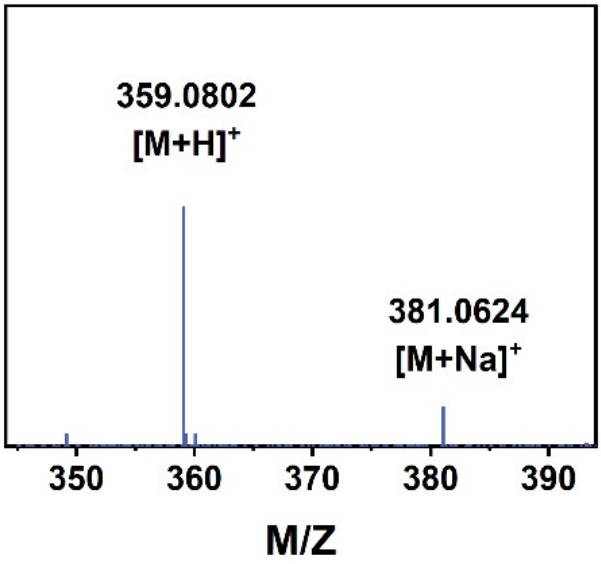

Figure S6. HRMS spectrum of COOH-Naph.

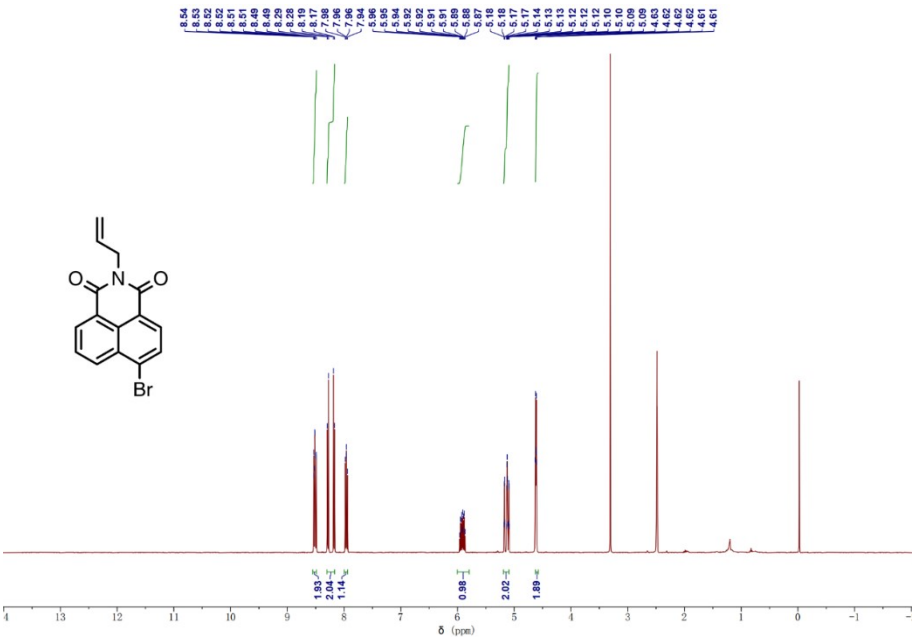

Figure S7. ^{1}H NMR spectrum of 2-allyl-6-bromo-1H-benzo[de]isoquinoline-1,3(2H)-dione (DMSO, 400 MHz, 298 K).

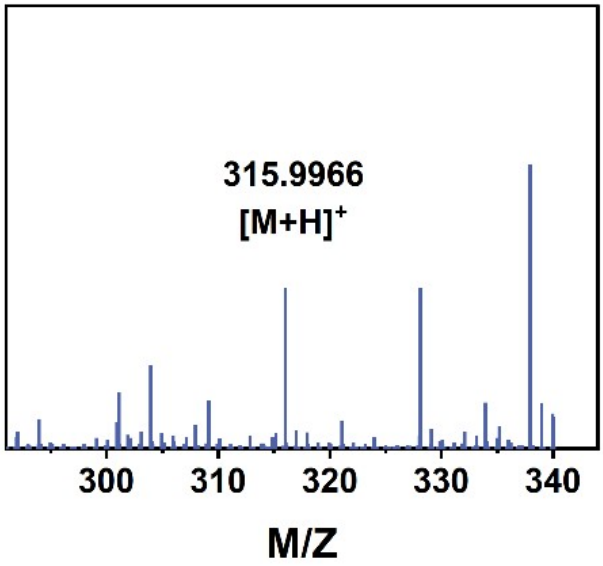

Figure S8. HRMS spectrum of 2-allyl-6-bromo-1H-benzo[de]isoquinoline-1,3(2H)-dione.

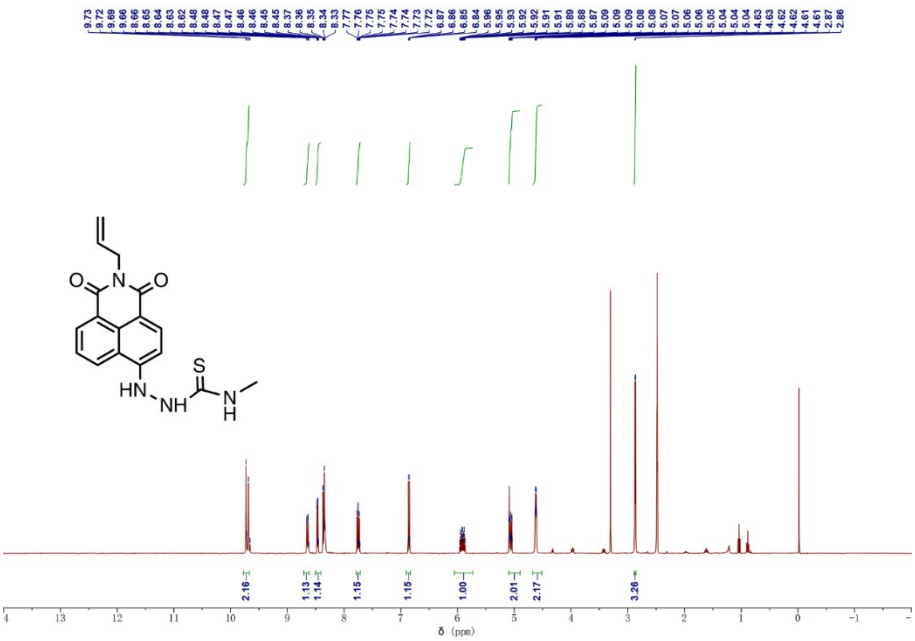

Figure S9. ^{1}H NMR spectrum of DB-Naph (DMSO, 400 MHz, 298 K).

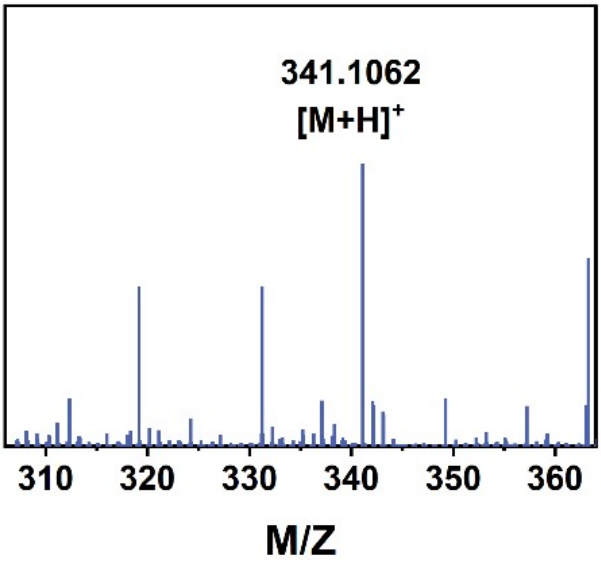

Figure S10. HRMS spectrum of DB-Naph.

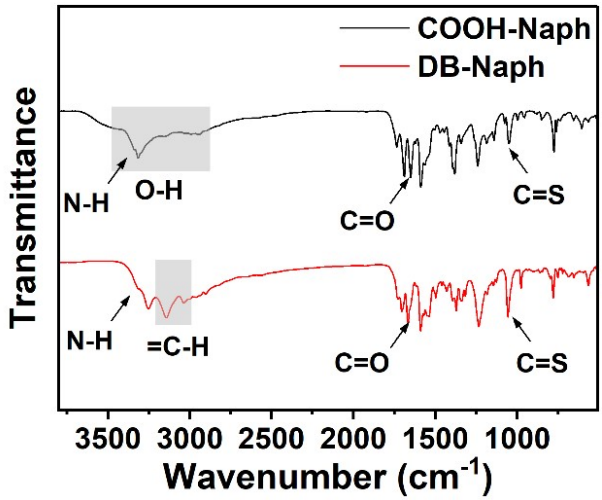

Figure S11. FTIR spectrum of COOH-Naph and DB-Naph.

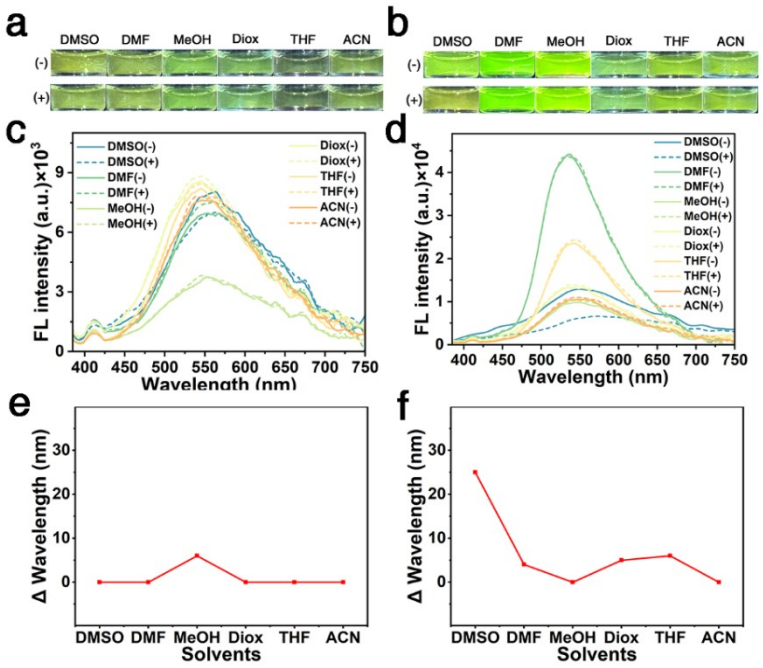

Figure S12. Fluorescence images under 365 nm illumination of (a) DB-Naph probe and (b) COOH-Naph probe in various solvents before and after adding EG-2201; Fluorescence spectra of (c) DB-Naph probe and (d) COOH-Naph probe in various solvents by before and after adding EG-2201; (e-f) corresponding wavelength shift before and after adding EG-2201.

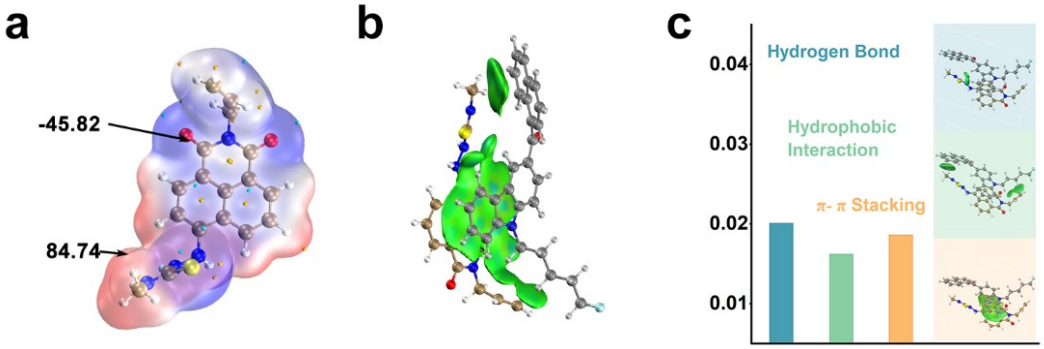

Figure S13. (a) ESP distribution of the DB-Naph probe, (b) IGM analysis for the interactions between the DB-Naph probe and EG-2201, and (c) corresponding δ(g) values for the specific interactions.

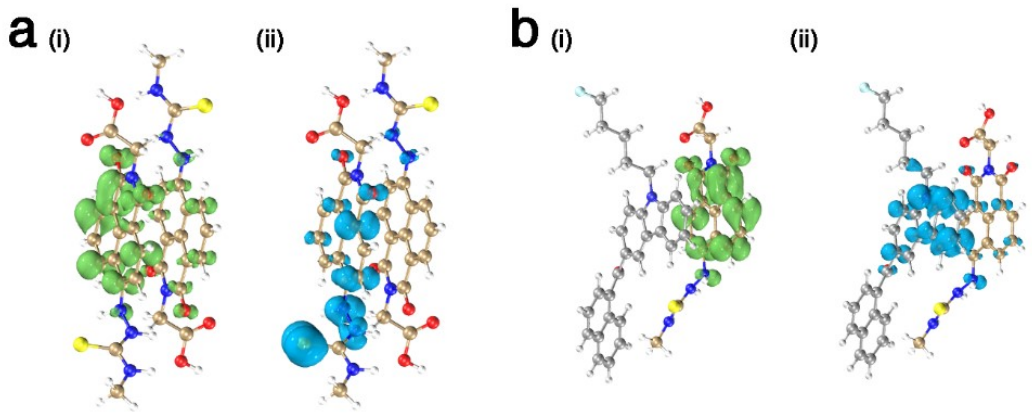

Figure S14. Distribution for the electron (in green) - hole (in blue) of (a) COOH-Naph dimer and (b) the complex of the COOH-Naph probe - EG-2201.

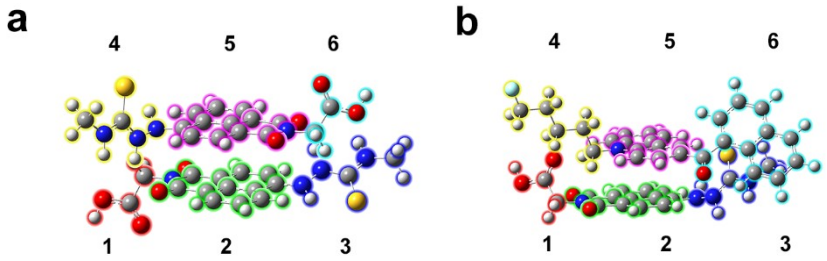

Figure S15. Fragmenting of (a) COOH-Naph dimer and (b) the complex of the COOH-Naph probe - EG-2201.

Note: The fragments 1-3 in (d-ii) correspond to carboxyl group, naphthalimide core and thiohydrazide group for one COOH-Naph probe molecule in the dimer, and the fragments 4-6 correspond to thiohydrazide group, naphthalimide core and carboxyl group for another COOH-Naph probe molecule in the dimer; the fragments 1-3 in (e-ii) correspond to carboxyl group, naphthalimide core and thiohydrazide group of the probe, and the fragments 4-6 correspond to 5-fluoropentyl group, carbazole core and naphthyl group of EG-2201 molecule.

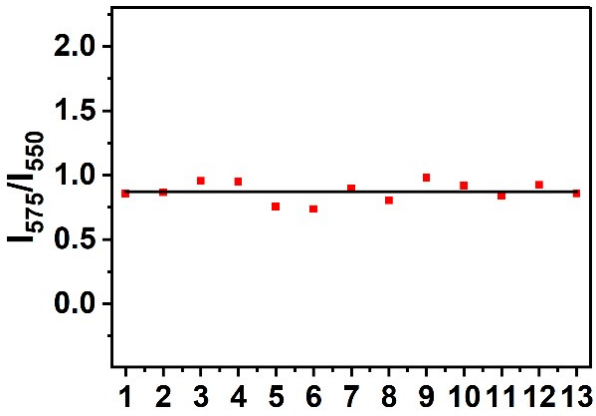

Figure S16. Signal fluctuation of the COOH-Naph probe solution (n=13).

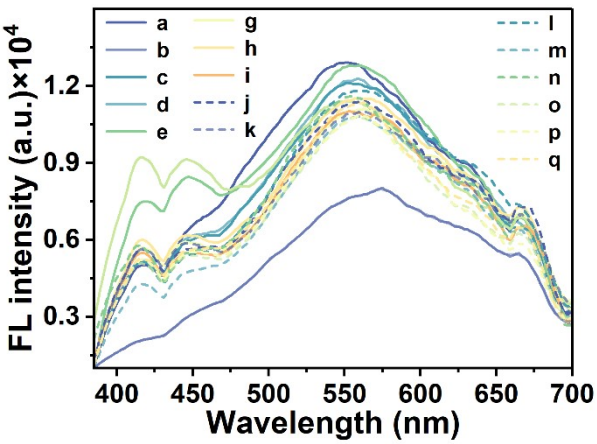

Figure S17. Fluorescence spectra of the COOH-Naph probe towards EG-2201 and analogues.

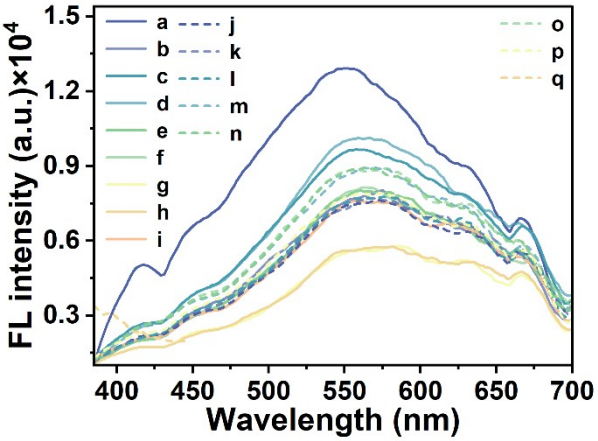

Figure S18. Fluorescence spectra of the COOH-Naph probe towards the mixture of EG-2201 and analogues.

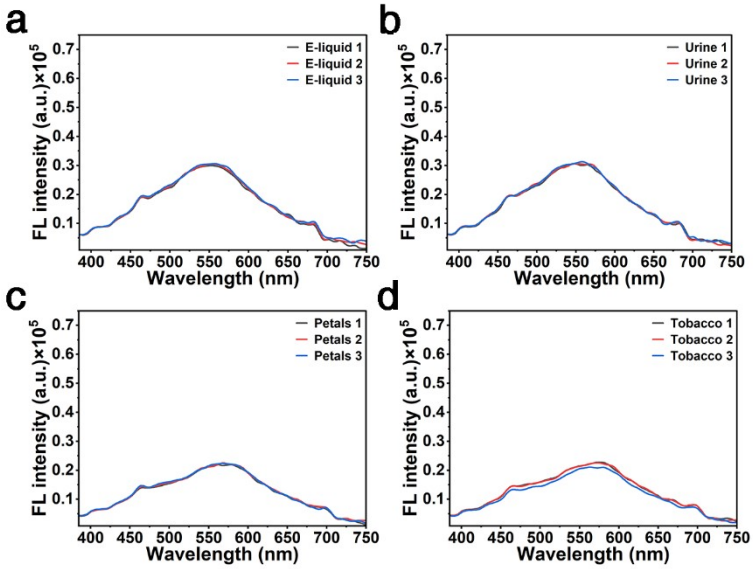

Figure S19. Fluorescence spectra of the spiked sample (a) E-liquid, (b) urine, (c) petals and (d) tobacco.

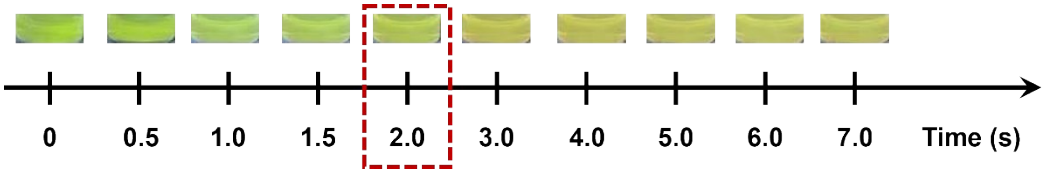

Figure S20. Response images of the COOH-Naph probe towards EG-2201 along with time change.

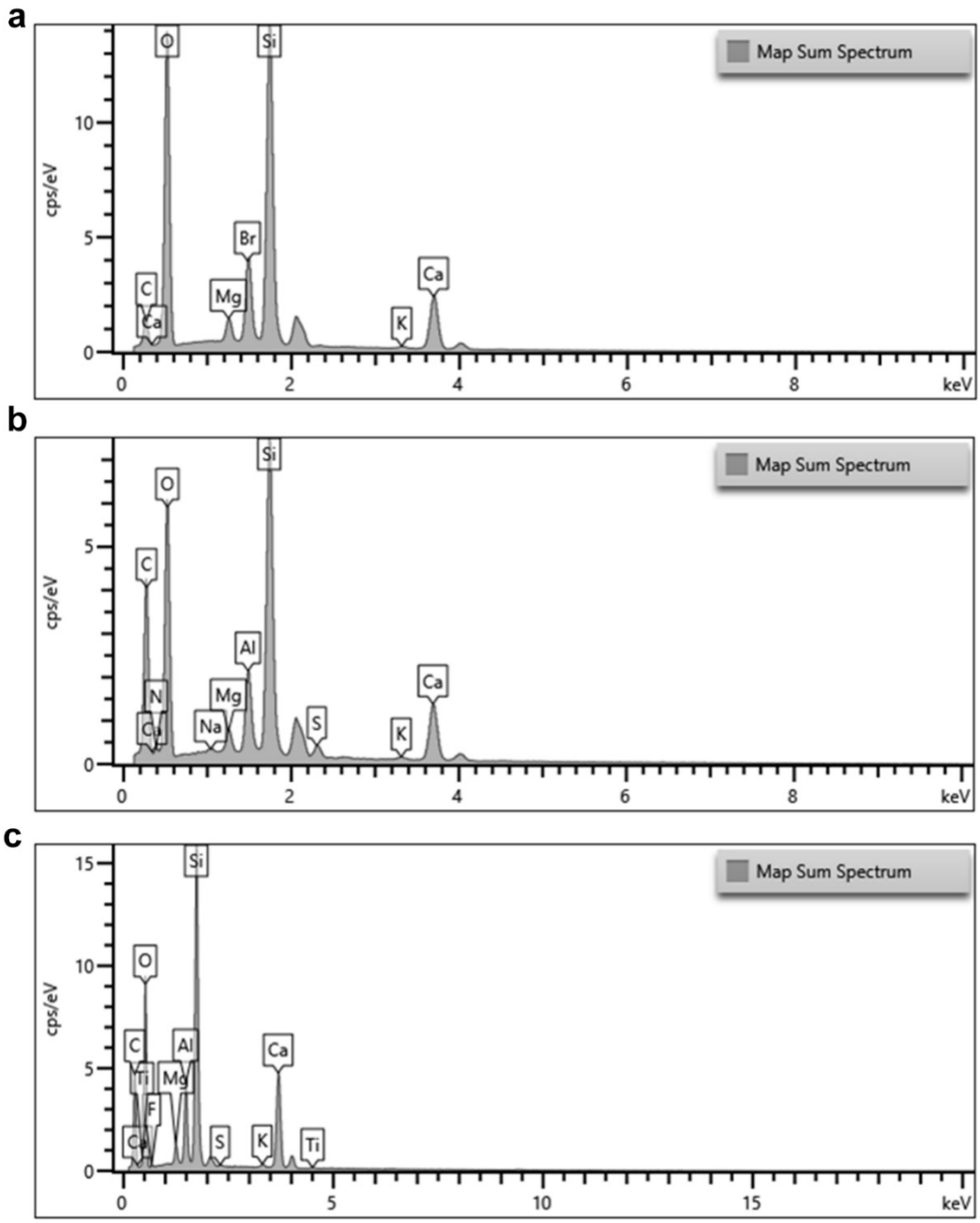

Figure S21. EDS data for (a) bare silicon-based fibrous film; functionalized sensing film (b) before and (c) after detecting EG-2201.

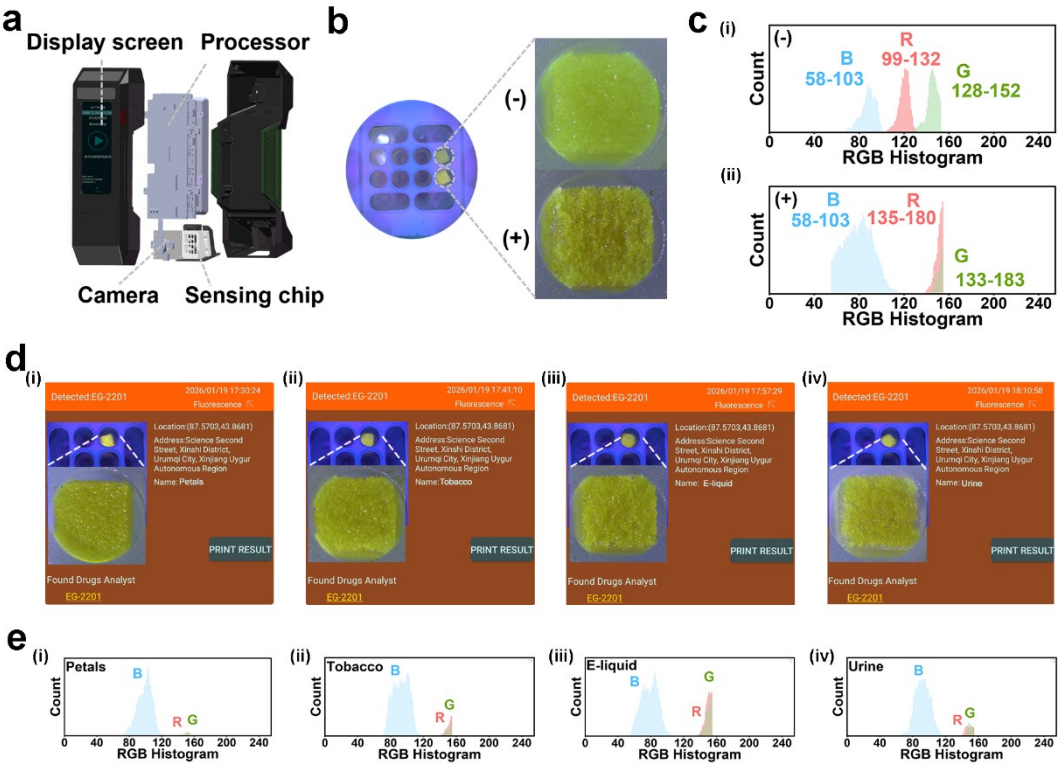

Figure S22. (a) Schematic illustration of the main frame structures for the home-made Drugs Analyst; (b) the probe functionalized polyurethane substrate (PU) placed in the sensing chip, the zoom-in images for the film before (-) and after (+) detecting EG-2201 (under 365 nm illumination); (c) the distributions of R, G, B values for the sensing images generated by Drugs Analyst before (-) and after (+) detecting EG-2201; (d) Sensing images and the displayed screens of the Drugs Analyst after detecting the real samples containing EG-2201; (e) the distributions of R, G, B values for the sensing images generated by Drugs Analyst after detecting EG-2201 in the real samples.

Note: The probe functionalized PU substrate also can be used for analyzing the EG-2201 existed in the complex mediums upon the combination with the intelligent Drugs Analyst. Upon the analysis of the HSV values and RGB distributions, the existence of EG-2201 can be precisely discriminated as below:

i) H value of the image in the HSV color model falls within the range of 50-67, the S value within 0.3-0.7, and the V value within 0.6-0.9, the sample would be identified to contain EG-2201; ii) In parallel, the R, G, B values of the sensing image in the presence of EG-2201 fell within the ranges of 135-180, 133-183 and 47-119, respectively, and a much more distinct overlap was observed between the R and G value distributions compared to the case in the absence of EG-2201.

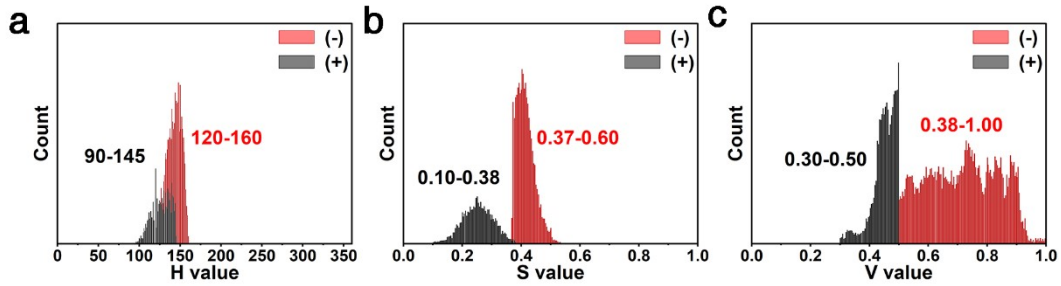

Figure S23. Distributions of H, S, V values for the sensing images generated by the integration of functionalized sensing film and Drugs Analyst before (-) and after (+) detecting EG-2201.

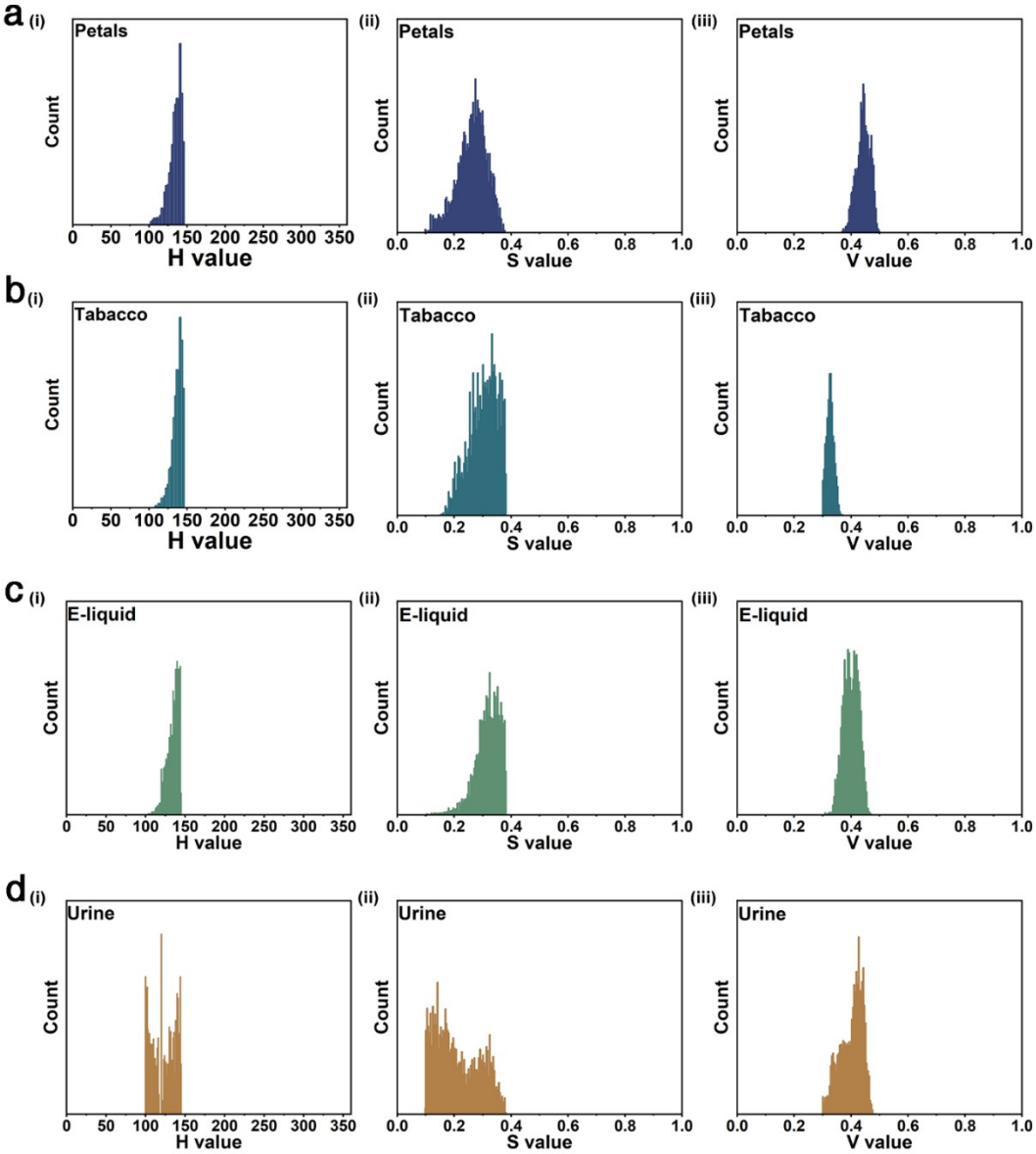

Figure S24. Distributions of H, S, V values for the sensing images generated by the integration of functionalized sensing film and Drugs Analyst before (-) and after (+) detecting EG-2201 in real samples.

3 Supplementary table

Table S1. Basic information of NPS.

Structural formulas	Abbreviations	IUPAC names	CAS numbers
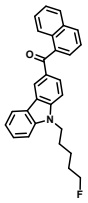	EG-2201	(9-(5-Fluoropentyl)-9H-carbazol-3-yl)(naphthalen-1-yl)methanone	2365471-72-1
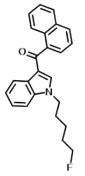	AM-2201	1-(5-Fluoropentyl)-3-(1-naphthoyl)indole	335161-24-5
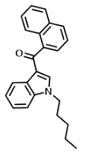	JWH-018	1-Pentyl-3- (1-naphthoyl) indole	209414-07-3
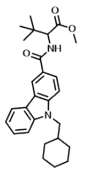	MDMB-CHMCZCA	Methyl 2-(9-(cyclohexylmethyl)-9H-carbazole-3-carboxamido)-3,3-dimethylbutanoate	2219324-32-8
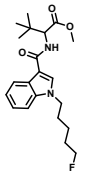	5F-MDMB-PICA	methyl 2-(1-(5-fluoropentyl)-1H-indole-3-carboxamido)-3,3-dimethylbutanoate	1971007-88-1
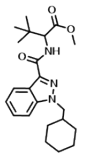	MDMB-CHMINCA	N-(1-Methoxy-3,3-dimethyl-1-oxobutan-2-yl)-1-(cyclohexymethyl)-1H-indazole-3-carboxamide	1715016-78-6
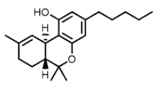	THC	(6aR,10aR)-6,6,9-trimethyl-3-pentyl-6a,7,8,10a-tetrahydro-6H-benzo[c]chromen-1-ol	1972-08-3
	Barbital	5,5-diethyl-1,3-diazinane-2,4,6-trione	57-44-3
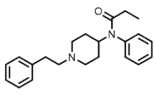	Fentanyl	N-phenyl-N-[1-(2-phenylethyl)piperidin-4-yl]propanamide	437-38-7

Table S2. Spike Recovery Results.

Sample name	EG-2201 Added (μM)	Measured concentration (μM)	Recovery (%)	Average Recovery (%)	RSD (%)
E-liquid 1	140.0	128.6	91.9		
E-liquid 2	140.0	132.1	94.4	95.4	4.1
E-liquid 3	140.0	140.0	100.0		
Urine 1	140.0	131.3	93.8		
Urine 2	140.0	143.4	102.4	98.0	4.3
Urine 3	140.0	136.8	97.7		
Petals 1	210.0	202.3	96.3		
Petals 2	210.0	203.8	97.0	95.2	2.5
Petals 3	210.0	194.1	92.4		
Tobacco 1	210.0	195.6	93.1		
Tobacco 2	210.0	194.0	92.4	93.2	0.3
Tobacco 3	210.0	197.9	94.2		

Table S3. Comparison of main performances for the recently developed analytical methods and this work regarding SCs detection.

Technique	Response time	Analyte	Linear range	LOD	Mixed Sample System	Ref
Fluorescence	-	JWH-018	12.5-100 μM	6.2 μM	Herbal mixtures	15
Colorimetry	-	AM-2201	17.39-208.68 μM	4.34 μM	Veronica，speedwell	16
Fluorescence	32 s	JWH-018	11-180 μM	11 μM	E-microdroplets	17
Fluorescence	5s	MDMB-CA series	800-2500 μM	22.3 μM	Urine, E-cigarette, tobacco	18
Fluorescence	10s	JWH-018	0-300 μM	2.16 μM	E-liquid, urea, artificial saliva, local sewage, cigarettes	19
Fluorescence	1.2 s	MDMB-type SCs	0-2.42 mM	4.35 μM	E-liquid, petals, tobacco, chocolate, popping candy	20
Fluorescence	2 s	EG-2201	114.0-260.5 μM	0.4 μM	E-liquid, urea, petals, tobacco	This work

4 References

[1] J. P. Perdew, K. Burke, M. Ernzerhof, *Physical Review Letters,* 1996, **77**, 3865.

[2] S. N. Maximoff, M. Ernzerhof, G. E. Scuseria, *Journal of Chemical Physics,* 2004, **120**, 2105.

[3] C. Adamo, V. Barone, *Journal of Chemical Physics,* 1999, **110**, 6158.

[4] S. Grimme, S. Ehrlich, L. Goerigk, *Journal of Computational Chemistry,* 2011, **32**, 1456.

[5] F. Weigend, R. Ahlrichs, *Physical Chemistry Chemical Physics,* 2005, **7**, 3297.

[6] T. Brinck, A. G. Larsen, K. M. Madsen, K. Daasbjerg, *Journal of Physical Chemistry B*, 2000, **104**, 9887.

[7] S. Miertuš, E. Scrocco, J. Tomasi, *Chemical Physics,* 1981, **55**, 117.

[8] J. D. Chai, M. Head-Gordon, *Physical Chemistry Chemical Physics,* 2008, **10**, 6615.

[9] J. D. Chai, M. Head-Gordon, *Journal of Chemical Physics,* 2008, **128**, 084106.

[10] M. J. Frisch, G. W. Trucks, H. B. Schlegel, G. E. Scuseria, M. A. Robb, J. R. Cheeseman, G. Scalmani, V. Barone, G. A. Petersson, H. Nakatsuji, X. Li, M. Caricato, A. V. Marenich, J. Bloino, B. G. Janesko, R. Gomperts, B. Mennucci, H. P. Hratchian, J. V. Ortiz, A. F. Izmaylov, J. L. Sonnenberg, D. Williams-Young, F. Ding, F. Lipparini, F. Egidi, J. Goings, B. Peng, A. Petrone, T. Henderson, D. Ranasinghe, V. G. Zakrzewski, J. Gao, N. Rega, G. Zheng, W. Liang, M. Hada, M. Ehara, K. Toyota, R. Fukuda, J. Hasegawa, M. Ishida, T. Nakajima, Y. Honda, O. Kitao, H. Nakai, T. Vreven, K. Throssell, J. A. Montgomery Jr., J. E. Peralta, F. Ogliaro, M. J. Bearpark, J. J. Heyd, E. N. Brothers, K. N. Kudin, V. N. Staroverov, T. A. Keith, R. Kobayashi, J. Normand, K. Raghavachari, A. P. Rendell, J. C. Burant, S. S. Iyengar, J. Tomasi, M. Cossi, J. M. Millam, M. Klene, C. Adamo, R. Cammi, J. W. Ochterski, R. L. Martin, K. Morokuma, O. Farkas, J. B. Foresman, D. J. Fox, Wallingford, CT, 2016.

[11] C. Lefebvre, G. Rubez, H. Khartabil, J. C. Boisson, J. Contreras-Garcia, E. Henon, *Physical Chemistry Chemical Physics,* 2017, **19**, 17928.

[12] T. Lu, F. Chen, *Journal of Computational Chemistry***,** 2012, **33**, 580.

[13] T. Lu, *Journal of Chemical Physics,* 2024, **161**, 082503.

[14] W. Humphrey, A. Dalke, K. Schulten, *Journal of Molecular Graphics & Modelling*, 1996, **14**, 33.

[15] Y. T. Yen, Y. J.Chang, Y. T. Tseng, C. Y. Chen, Y. L. Liu, H. T. Chang, *Sensors and Actuators B: Chemical,* 2022, **353**, 131151.

[16] D, Hasan, D. Selen, Ü. Aysem, G. Bahar, E. Erol, A. Resat, *Analytical Sciences,* 2018**, 34***,* 1419.

[17] C. Liu, F. Xiao, Y. Li, D. Lei, Y. Liu, X. Ma, C. Gu, X. Dou, *Aggregate*, 2023, **4**, 4.

[18] Y. Wang, J. Dong, Y. Liu, L. Liang, Y. Du, X. Dou, *Angewandte Chemie International Edition*, 2025, **64**, 17.

[19] Y. Feng, L. Yang, Y. Li, C. Zhao, N. Yisimayili, J. Yang, X. Dou, B. Zu, *Analytical Chemistry*,

2025, **97**, 17615.
[20] B. Chen, Y. Li, C. Zhao, Y. Liu, Y. Du, N. Wang, M. Guan, X. Dou, *Analytical Chemistry*, 2025, **97**, 11589.